

Article

Synchronization of an On-Board Photovoltaic Converter Under Conditions of High Dynamic Voltage Frequency Change

Tomasz Binkowski ^{1,*}, Ľubomír Beňa ², Dušan Medved' ² and Paweł Pijarski ³

¹ Department of Power Electronics and Power Engineering, Faculty of Electrical and Computer Engineering, Rzeszow University of Technology, Al. Powstańców Warszawy 12, 35-959 Rzeszów, Poland

² Department of Electric Power Engineering, Faculty of Electrical Engineering and Informatics, Technical University of Kosice, Letna 9, 042 00 Kosice, Slovakia; lubomir.bena@tuke.sk (L.B.); dusan.medved@tuke.sk (D.M.)

³ Department of Power Engineering, Faculty of Electrical Engineering and Computer Science, Lublin University of Technology, Nadbystrzycka St. 38D, 20-618 Lublin, Poland; p.pijarski@pollub.pl

* Correspondence: tbinkow@prz.edu.pl

Abstract: The decarbonization of energy systems is forcing the development of renewable energy generation and consumption technologies. Photovoltaic systems are being used in almost every industry, including autonomous power systems used on ships, space vehicles, or flying platforms, where the voltage supplying specific equipment can change in an overridingly controlled manner. Feeding energy from a renewable source into a power system with highly dynamic frequency changes is not possible for traditional grid converter control strategies. This is caused by the synchronization system, which is designed for a fixed value of the grid voltage frequency, and by the proportional-resonant controllers used. In this paper, it is shown that frequency tracking correction causes deviations from the unit amplitude of synchronization signals, causing errors in the reference signals responsible for the active and reactive components of the converter current. To solve this problem, a new variable frequency adaptation system using a generalized second-order integrator was proposed. As a result, synchronization signals of unit amplitude were obtained. Due to the proposed method, the proportional-resonant controller was able to control the active and reactive components of the current even when the voltage frequency changes, adjusting the resonant frequency.

Keywords: synchronization; variable frequency; photovoltaic; proportional-resonance control



Citation: Binkowski, T.; Beňa, Ľ.; Medved', D.; Pijarski, P. Synchronization of an On-Board Photovoltaic Converter Under Conditions of High Dynamic Voltage Frequency Change. *Energies* **2024**, *17*, 6302. <https://doi.org/10.3390/en17246302>

Academic Editor: Frede Blaabjerg

Received: 16 November 2024

Revised: 10 December 2024

Accepted: 11 December 2024

Published: 13 December 2024



Copyright: © 2024 by the authors. Licensee MDPI, Basel, Switzerland. This article is an open access article distributed under the terms and conditions of the Creative Commons Attribution (CC BY) license (<https://creativecommons.org/licenses/by/4.0/>).

1. Introduction

A stable energy future is the main goal of the research that is being carried out in the field of energy conversion. The decarbonization of power systems is becoming a global effort that requires large-scale implementation of zero-carbon technologies [1], particularly for the generation of renewable energy. Photovoltaic (PV) and wind power plants are now cost competitive with power generation from fossil fuel sources. Interest in low-carbon technologies is gaining momentum and is expanding into larger and larger operating areas. One such area is the facility with autonomous power grids, designed and customized to meet specific energy requirements. Examples include space vehicles or shipboard systems.

In the case of facilities containing autonomous power supply systems, an essential component of power generation is a system of generators, often powered by engines fueled by fossil fuels. Synchronized generator operation is the basis for the stability of the internal grid and the key to preventing unwanted power outages. In the situation of using renewable energy sources, the problem is complicated by the voltage inverters connected to the on-board grid, which are an essential element for the integration with renewable energy resources. Complication arises from the need for perfect synchronization of power control algorithms with voltages in the grid, without which maintaining acceptable reliability and efficiency of power systems becomes a difficult, and in some situations impossible, task [2].

The use of power electronic systems, especially converters connected to the grid, requires proper synchronization with the frequency and phase of the voltage of the grid. This is a critical task for the correct operation of synchronous-based controllers due to their dependence on the accuracy of variable transformation procedures [3–5]. Extensive research into the methods of synchronizing grid converters reduces to procedures for minimizing deviations in voltage, phase angle, and frequency between the output of a renewable energy source generator and the grid [6].

The most popular synchronization schemes for grid-connected inverters are based on phase locked loop (PLL) and extended PLL (EPLL) [7–12]. Among the techniques described in the literature, solutions based on Kalman filtering [13–16] and discrete or recursive Fourier transforms can be found [17–19]. These methods are able to provide control algorithms not only with the information necessary for synchronization but also with information regarding harmonics. Thanks to them, it is possible to activate procedures to improve the quality of electricity in the power system. One of the most commonly used methods of synchronization in single-phase systems is also a method based on the use of a generalized second-order integrator (SOGI), which performs harmonic detection and generates the necessary synchronization signals [20–22]. With SOGI, synchronization systems characterized by low complexity in relation to methods using Fourier transform or Kalman filters are obtained.

The synchronization methods described in the literature refer to power grids with fixed voltage frequency. In the case of autonomous on-board grids, the voltages have a wide frequency range reaching up to 800 Hz. In such a situation, the estimation of synchronization signals is a more difficult problem [23] than in the case of typical power grids. This is caused by problems in the accuracy of the calculations that cause a reduction in the dynamic response of the synchronization system in the estimation of voltage parameters. All described synchronization methods are characterized by good performance in estimating voltage parameters only around the equilibrium point [24]. The work [18,25] attempted to estimate the frequency of the change in a system designed for aircrafts, but its main weakness is the high computational load. This article focuses mainly on the problem of synchronization using the PLL technique. This is the most widely used synchronization technique, broadly described in the literature and with many improvements and modifications. However, it should be particularly emphasized that the PLL technique used in grid converters applies to cases where the grid voltage has a constant frequency. In such a situation, it is possible to properly design filters that make the PLL synchronization perform perfectly in the characteristic frequency environment. In the case of large frequency changes, this technique is no longer useful. Even knowing the function of frequency changes, modifying the characteristic frequency on the fly in the PLL algorithm will result in the errors in synchronization signals. If the dynamics of frequency changes is not large, these errors can be ignored, while at high dynamics, these errors will already be significant. In the system described in this paper, the high dynamics of frequency changes is characteristic and necessary for proper operation of the device. Therefore, to control the active and reactive power, it was necessary to change the synchronization process that led to a circular trajectory of orthogonal components responsible for the reference values of the active and reactive current.

Many on-board grids are characterized by the presence of power buses with different voltage parameters. Typical AC sub-grids are characterized by different voltage parameters, in particular different voltage frequencies in relation to the objects fed from them. In most cases, the voltage parameters of these buses are fixed, and the connection of grid converters that integrate them with renewable energy sources requires the use of known synchronization methods, effectively estimating the voltage parameters around static equilibrium points. A special group is represented by power buses, which are connected devices that require dynamic changes in the value of voltage amplitude or frequency. An example of such a device can be an ozone generator, which is necessary in water treatment processes. In such a situation, the use of classical synchronizers becomes impossible

because of the wide divergence of the device's operating frequency from the synchronizer's equilibrium point. The main challenge of the work was to develop a new synchronization system which, by modifying to an adaptive form of a generalized second-order integrator, allows efficient synchronization of a grid converter with a widely varying grid frequency. Consequently, this allows precise control of the active and reactive components of the current of the grid without causing emergency shutdowns of the device.

The rest of this paper is organized as follows. Section 2 describes the synchronization problem resulting from linear changes in the frequency and amplitude of the supply voltage. The problem resulting from a voltage having the shape of a chirped signal is analytically demonstrated, and the numerically determined error causing disturbance of the control system's reference signals is presented. A new algorithm for adaptive synchronization and a proportional-resonant control system is described. Section 3 presents test results that confirm the effectiveness of the proposed method. Section 4 concludes this paper by formulating the final conclusions.

2. Materials and Methods

The vast majority of systems in which energy is converted operate at constant operating parameters. If these parameters change over time, these changes usually have time constants that are many times larger than the characteristic time constants of the converter devices. However, there are situations in which the given trajectories of changes in operating parameters are characterized by high dynamics, which cause disturbances in the operation of the converter. One such device is an ozone generator, used in the water treatment process. The processes of optimizing energy distribution and consumption on flying platforms, ships, and space vehicles also require the use of renewable energy. This study refers to the analysis of the use of solar energy in the ozone production process in the context of changes in the high dynamics of voltage frequency forcing internal electrical discharges. The system shown in the block diagram in Figure 1 was tested.

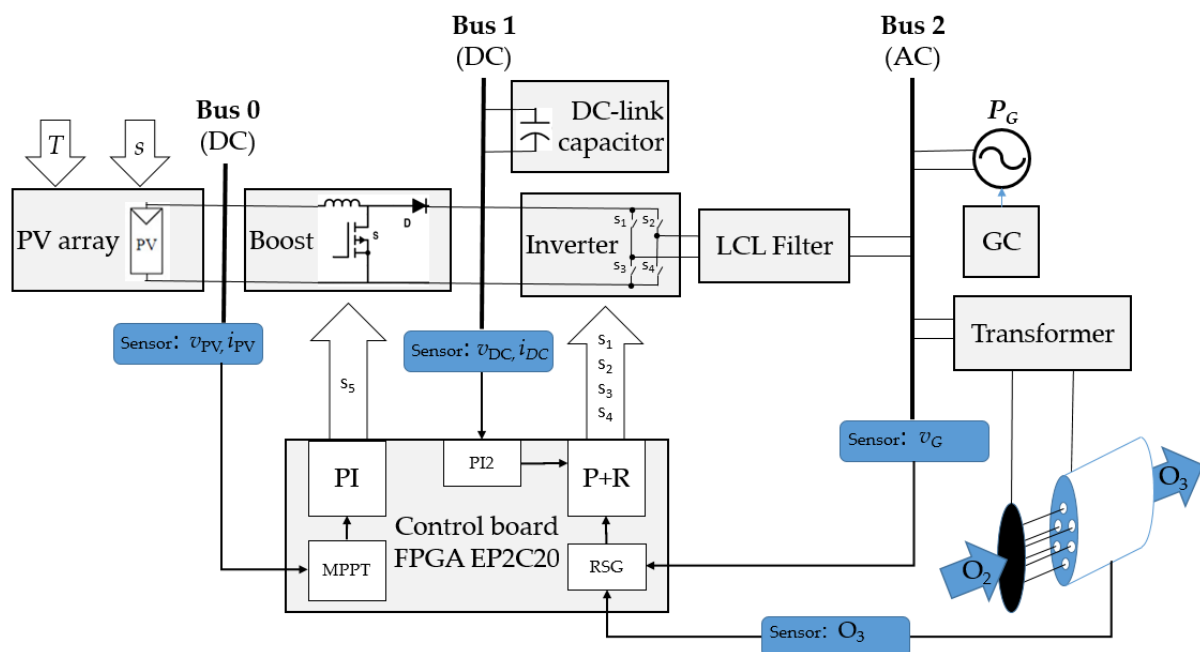


Figure 1. Block diagram of a photovoltaic converter system connected to an alternating-current voltage bus of variable frequency.

The tested system is part of an on-board system developed and reported in publications [26], in which the solar energy conversion subsystem is connected to Bus 2. Bus 2 supplies power to a facility characterized by a high-step voltage frequency trajectory during the start-up phase. It was assumed that the trajectory of changes in the voltage

generator’s operating parameters is made independently through the system (GC) controlling the operation of the power generator (PG). In the research conducted, the device start process was assumed by implementing a reference voltage trajectory according to the curves shown in Figure 2.

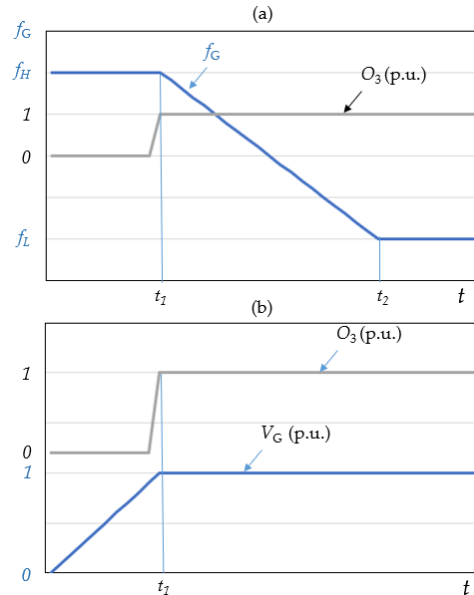


Figure 2. Trajectories of changes in frequency (a) and amplitude (b) of voltage at the point of connection of the grid converter.

At the time of starting the device, the generator starts to operate with a voltage at the maximum frequency f_H and amplitude close to zero. By linearly increasing the voltage at a constant frequency, the start-up control process waits for the signal of the beginning of electrical discharges in the device and the production of ozone. When the initiated ozone production process is detected (t_1), the generator starts to reduce the voltage frequency from f_H to f_L . This reduction occurs linearly and lasts until the moment (t_2), defined in the technological process as the stable phase. An example of the Bus 2 voltage waveform of a generator implementing the assumed trajectory of amplitude and frequency changes is shown in Figure 3.

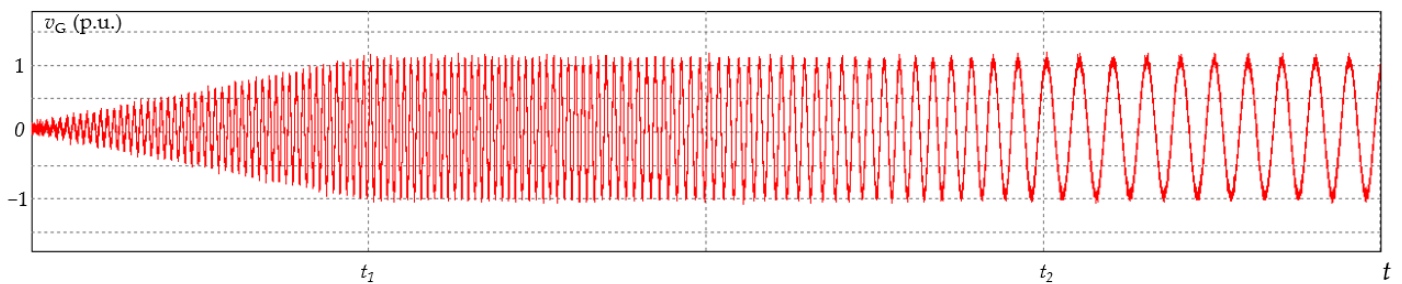


Figure 3. Generator voltage waveform at the connection point of the grid converter.

Taking into account the voltage frequency trajectory from Figure 2a and the voltage amplitude trajectory from Figure 2b, the voltage waveform v_G on Bus 2 can be described as follows.

$$v_G(t) = \begin{cases} \frac{V}{t_1} t \sin(2\pi f_H t) & \text{for } t \leq t_1 \\ V \sin\left(2\pi \frac{f_H - f_L}{t_1 - t_2} t^2 + 2\pi \frac{f_L t_1 - f_H t_2}{t_1 - t_2} t\right) & \text{for } t_1 < t \leq t_2 \\ V \sin(2\pi f_L t) & \text{for } t > t_2 \end{cases} \quad (1)$$

where V is the amplitude of the voltage at which sliding discharges occur.

Assuming that the energy needed to generate ozone comes not only from the generator (PG), but also from the photovoltaic panels, a photovoltaic converter is connected to Bus 2 to transmit the converted solar energy. The amount of energy available depends on environmental parameters such as the outdoor temperature T and the solar irradiance s , and is a function of the installed power of the PV. The operating point of photovoltaic panels is determined by the Maximum Power Point Tracker (MPPT) that implements the incremental conductance algorithm [27] based on the current values of the photovoltaic voltage v_{PV} and the photovoltaic current i_{PV} . In the proportional integral control algorithm (PI), the fill factor is determined for the switch s in the boost converter. This converter controls the capacitor charge current in the DC link in a way that allows the maximum power point of the PV to be obtained. Increasing or decreasing the current feed into the DC link causes the voltage across Bus 1 to rise or fall, respectively. To counteract this, based on the measured voltage value in Bus 1, another proportional integral regulator (PI2) controls the reference current of the grid converter (inverter), leading to voltage stabilization in Bus 1.

The value of the current fed by the grid converter into Bus 2 depends on the current energy production of the PV. Most of the time, the grid inverter is not loaded with nominal power, so it was used to compensate for the reactive power in Bus 2. The parameters of the current fed into Bus 2 are determined by the proportional-resonant regulator (P + R), which controls the active and reactive components of the current. This is possible only if the current control algorithm has current information on the orthogonal components of the voltage v_C occurring on Bus 2. The function of the orthogonal signal generator is performed by the reference shape signal generator (RSG).

The proportional-resonant control system that controls the current fed Bus 2 is designed to directly control the active and reactive components. The reference value of the active component i_{ar} is set to obtain a stable voltage on Bus1 according to Formula (2).

$$i_{ar}(t) = k_P \cdot \Delta v_{DC} + \frac{1}{T_C} \int \Delta v_{DC} dt, \quad (2)$$

where Δv_{DC} is the voltage deviation on Bus 1, k_P is the gain and T_C is the integration constant. The reference value of the reactive component i_{rr} is arbitrarily determined based on the given level of reactive power compensation on Bus 2. The calculated active and reactive components of the current are used to define the reference waveform for the proportional-resonant algorithm according to Formula (3).

$$i_r(t) = i_{ar}(t) \cdot \hat{v}_q(t) + i_{rr}(t) \cdot \hat{v}(t), \quad (3)$$

where \hat{v}_q and \hat{v} estimate the cosine and sine components of the voltage on Bus 2, respectively. In the case of ac systems characterized by a constant voltage frequency, the waveforms of the sinusoidal and cosine components of the voltage can be easily calculated using the known structures of quadrature generators based on the integration of the fundamental component obtained from the phase lock loop (PLL) system. In the case of the voltages described by Equation (1), there is a problem related to the calculation of the combination of the trigonometric function and the linear function.

Assuming that in the linear stage of the voltage frequency change, the fundamental component estimation algorithm (implemented in RSG) reconstructs it by directly implementing the trajectory in the form of Equation (4):

$$f(t) = a_f \cdot t, \quad (4)$$

where a_f is the is a directional coefficient that determines the dynamics of frequency changes, the reference signal curve can be written in the form (5):

$$\hat{v}(t) = \sin(2\pi f(t)t) = \sin(2\pi a_f t^2). \quad (5)$$

Formula (5) describes a typical chirp signal in which the frequency increases (for $a_f > 0$) or decreases (for $a_f < 0$) over time. It is commonly used in spread spectrum systems. To analyze the influence of the voltage estimate given by Equation (5) on the control process, its transform should be analyzed. The Fourier transform of the following function (5) has the form:

$$\mathcal{F}\{\sin(2\pi a_f t^2)\}(\omega) = \int_{-\infty}^{\infty} \sin(2\pi a_f t^2) e^{-i\omega t} dt \quad (6)$$

The function (5) can be written as

$$\sin(2\pi a_f t^2) = \frac{e^{i2\pi a_f t^2} - e^{-i2\pi a_f t^2}}{2i}, \quad (7)$$

then

$$\mathcal{F}(\omega) = \frac{1}{2i} \left(\int_{-\infty}^{\infty} e^{i2\pi a_f t^2} e^{-i\omega t} dt - \int_{-\infty}^{\infty} e^{-i2\pi a_f t^2} e^{-i\omega t} dt \right) = \frac{1}{2i} \left(\int_{-\infty}^{\infty} e^{i(2\pi a_f t^2 - \omega t)} dt - \int_{-\infty}^{\infty} e^{-i(2\pi a_f t^2 + \omega t)} dt \right) \quad (8)$$

Due to the fact that the exponents in Equation (8) are quadratic functions, the resulting oscillating integrals can be simplified by substituting:

$$\phi_1(t) = 2\pi a_f t^2 - \omega t, \quad (9)$$

$$\phi_2(t) = 2\pi a_f t^2 + \omega t. \quad (10)$$

Assuming a stationary point where the phase differential takes a value of zero, the results are obtained:

$$\frac{d\phi_1(t)}{dt} = 4\pi a_f t - \omega = 0 \Rightarrow t = \frac{\omega}{4\pi a_f}, \quad (11)$$

and

$$\frac{d\phi_2(t)}{dt} = 4\pi a_f t + \omega = 0 \Rightarrow t = -\frac{\omega}{4\pi a_f}. \quad (12)$$

The Fourier transform of a quadratic phase function leads to a result proportional to the Gaussian function in the frequency domain. On the basis of the symbolic calculations performed in Maple, approximate results were obtained:

$$\mathcal{F}\{e^{i2\pi a_f t^2}\}(\omega) \approx \sqrt{\frac{1}{2a_f}} e^{-\frac{\omega^2}{8\pi a_f}} e^{i\frac{\pi}{4}}, \quad (13)$$

and

$$\mathcal{F}\{e^{-i2\pi a_f t^2}\}(\omega) \approx \sqrt{\frac{1}{2a_f}} e^{-\frac{\omega^2}{8\pi a_f}} e^{-i\frac{\pi}{4}}. \quad (14)$$

By substituting (13) and (14) into (8), it can be written:

$$\mathcal{F}(\omega) = \frac{1}{2i} \left(\sqrt{\frac{1}{2a_f}} e^{-\frac{\omega^2}{8\pi a_f}} e^{i\frac{\pi}{4}} - \sqrt{\frac{1}{2a_f}} e^{-\frac{\omega^2}{8\pi a_f}} e^{-i\frac{\pi}{4}} \right). \quad (15)$$

Assuming a constant value for the steepness of the frequency ramp a_f , the Fourier transform (15) can be simplified to the form:

$$\mathcal{F}(\omega) = \sqrt{\frac{1}{2a_f}} e^{-\frac{\omega^2}{8\pi a_f}} \left(\frac{e^{i\frac{\pi}{4}} - e^{-i\frac{\pi}{4}}}{2i} \right) = \sqrt{\frac{1}{2a_f}} e^{-\frac{\omega^2}{8\pi a_f}} \sin\left(\frac{\pi}{4}\right) = \sqrt{\frac{1}{4a_f}} e^{-\frac{\omega^2}{8\pi a_f}}. \quad (16)$$

Formula (16) is in the form of a Gaussian function with a distribution that depends on the rate of frequency change. Therefore, it can be concluded that as a function of the steepness of frequency changes in the interval from t_1 to t_2 , the amplitude of the signal estimate described by Equation (5) will change. In this case, the use of a standard PLL will cause the reference waveforms obtained in it to be no longer unit waveforms.

In a further stage of research, the problem arising from Equation (16) was analyzed in the structure of a generalized second-order integrator, which acts as a quadrature generator for phase synchronization. The equations of the quadrature generator are described by the following equations:

$$\frac{d^2\hat{v}}{dt^2} + \omega \frac{d\hat{v}}{dt} + \omega^2 = \omega \frac{dv}{dt} \quad (17)$$

$$\frac{d^2\hat{v}_q}{dt^2} + \omega \frac{d\hat{v}_q}{dt} + \omega^2 = \omega^2 v \quad (18)$$

where \hat{v} and \hat{v}_q are orthogonal signals, v is the input signal and $\omega = 2\pi f$. The Bode plots corresponding to Equations (17) and (18) are shown in Figure 4.

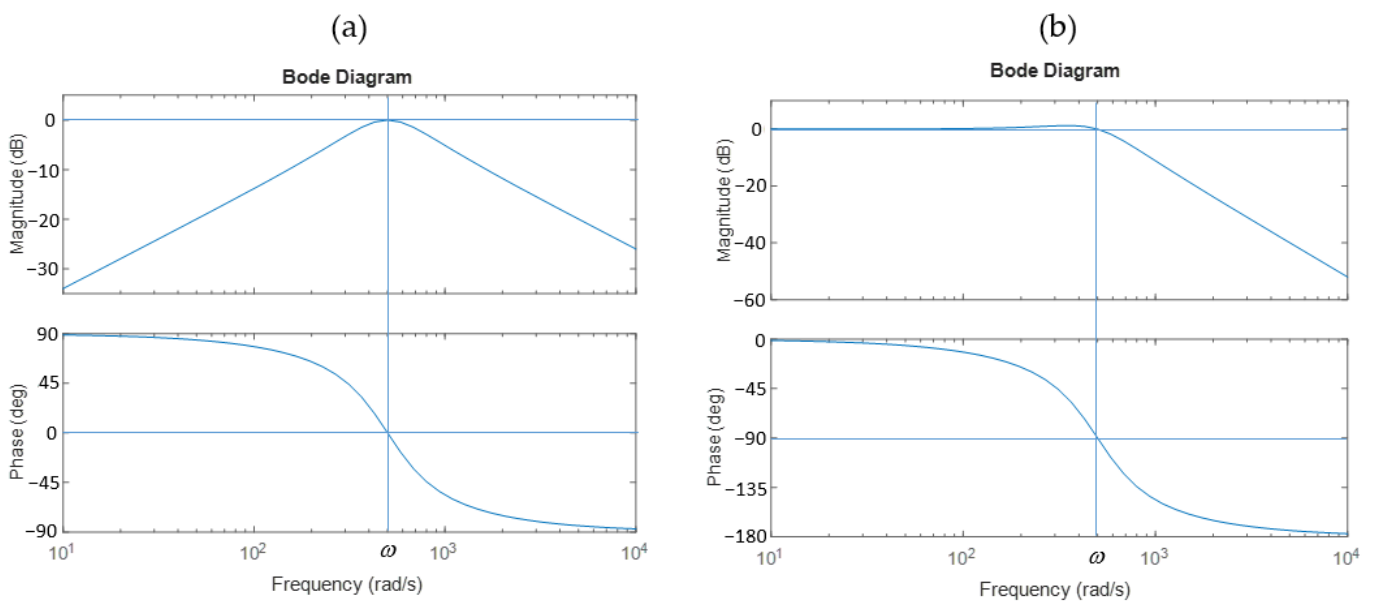


Figure 4. Bode plots of the generalized second-order integrator for frequency $f = 500$ Hz: signal of the fundamental component \hat{v} (a); signal of the orthogonal component \hat{v}_q (b).

Figure 4a shows the Bode plot of the sine function, and Figure 4b the cosine function determined for a fixed frequency $\omega = 500$ Hz. Analyzing the plots, it can be concluded that for a variable frequency, the sinusoidal signal should be disturbed to a small degree relative to the cosine signal. In the case of the chirp signal, which occurs in the interval from t_1 to t_2 of the signal presented in Figure 3, Equations (17) and (18) can be written in the form:

$$\frac{t_1 - t_2}{2\pi((f_H - f_L)t + f_L t_1 - f_H t_2)} \frac{d^2\hat{v}}{dt^2} + \frac{d\hat{v}}{dt} + 2\pi((f_H - f_L)t + f_L t_1 - f_H t_2) = \frac{dv}{dt} \quad (19)$$

$$\frac{t_1 - t_2}{4\pi^2((f_H - f_L)t + f_L t_1 - f_H t_2)^2} \frac{d^2\hat{v}_q}{dt^2} + \frac{1}{2\pi((f_H - f_L)t + f_L t_1 - f_H t_2)} \frac{d\hat{v}_q}{dt} + 1 = v \quad (20)$$

The analytical solution of differential Equations (19) and (20) is a complex problem, so their numerical simulation was performed. The block structure of the equations that describe the quadrature signal generator based on the second-order generalized integrator with linearly variable frequency is shown in Figure 5.

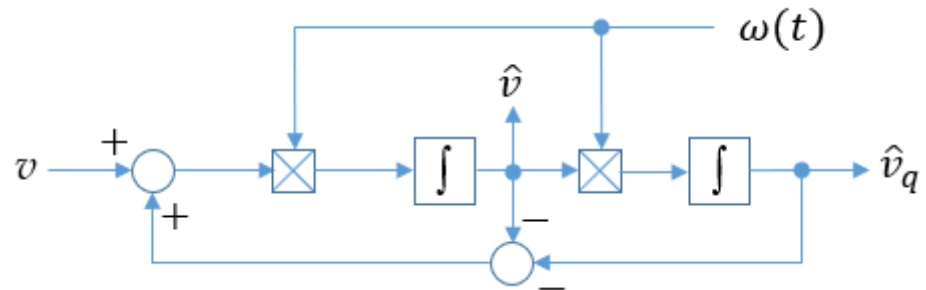


Figure 5. Block structure of the generalized second-order integrator.

During the test, it was assumed that the input signal v is in the form of a fixed frequency signal $f_H = 500$ Hz, which at time t_1 changes into a chirped signal with a linear modulated frequency. The linear frequency modulation ends at time t_2 , when the frequency of the chirped signal reaches $f_L = 100$ Hz. The waveforms of the input signal applied to the generalized second-order integrator and the frequency change profile are shown in Figure 6.

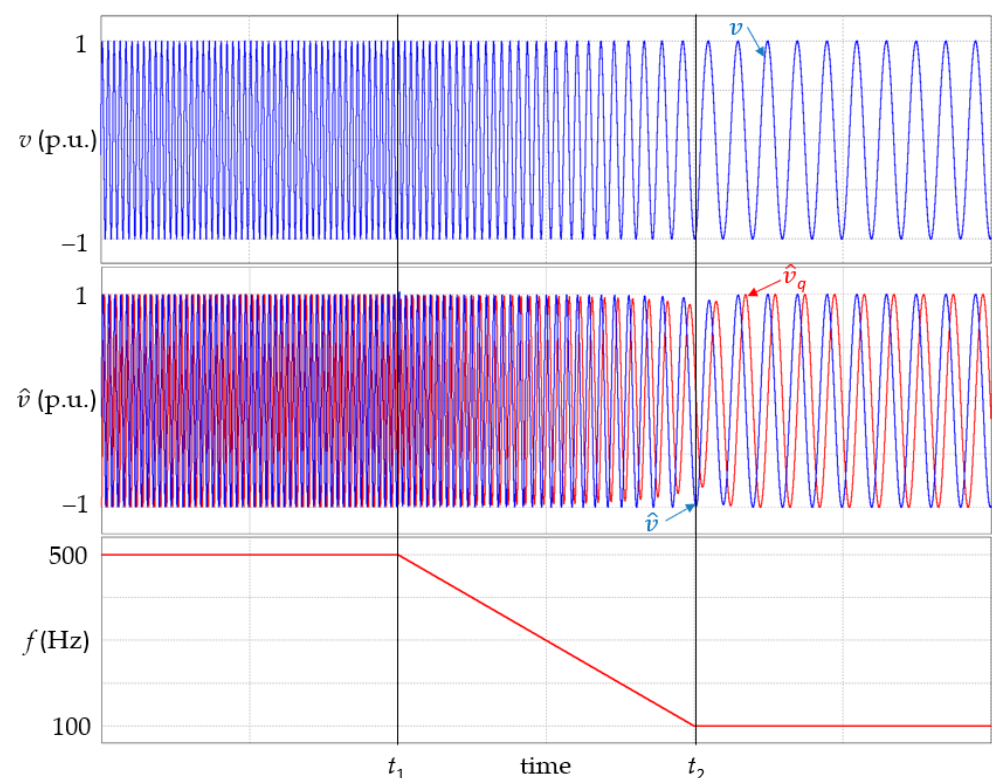


Figure 6. The voltage waveform v and the quadrature signal estimates \hat{v} and \hat{v}_q obtained by direct implementation of the frequency variation profile f in the generalized second-order integrator.

To obtain quadrature signals based on the generalized second-order integrator shown in Figure 5 it is necessary to include the frequency value in the signal processing. If the frequency changes, the Bode plots cannot be analyzed due to the fact that frequency is a fixed transmittance parameter. These signals can only be calculated from Equations (19) and (20). In the case of a frequency change according to a known profile $\omega(t)$, the profile can be inserted into the calculation instead of the fixed parameter. If a frequency variation profile

is substituted for a fixed parameter, calculations will be performed to continuously update its value. Intuitively, it may seem that, as a consequence of this update of frequency values, orthogonal signals should be correctly estimated. In Figure 6, it can be observed that the calculated quadrature signals correctly track the frequency changes, but their amplitudes change as the input signal is reduced. This observation confirms the conclusions formulated for Equations (19) and (20).

Properly estimated quadrature signals should be sinusoidal and have unit amplitude. In the case of the analyzed frequency variation profile, the trajectory resulting from the quadrature signals should always be a circle with a unit radius. Figure 7 shows the trajectories resulting from the calculations of the generalized second-order integrator for a fixed frequency, corresponding to the initial frequency f_H and the final frequency f_L . Analysis of the obtained trajectories shows the change from circular to elliptical form or vice versa, remaining circular only for the frequency interval consistent with the set parameter. The densities of the paths of the elliptical envelope trajectory indicate at the same time the achievement of a steady state characterized by a non-unit amplitude value and non-orthogonality of the waveforms.

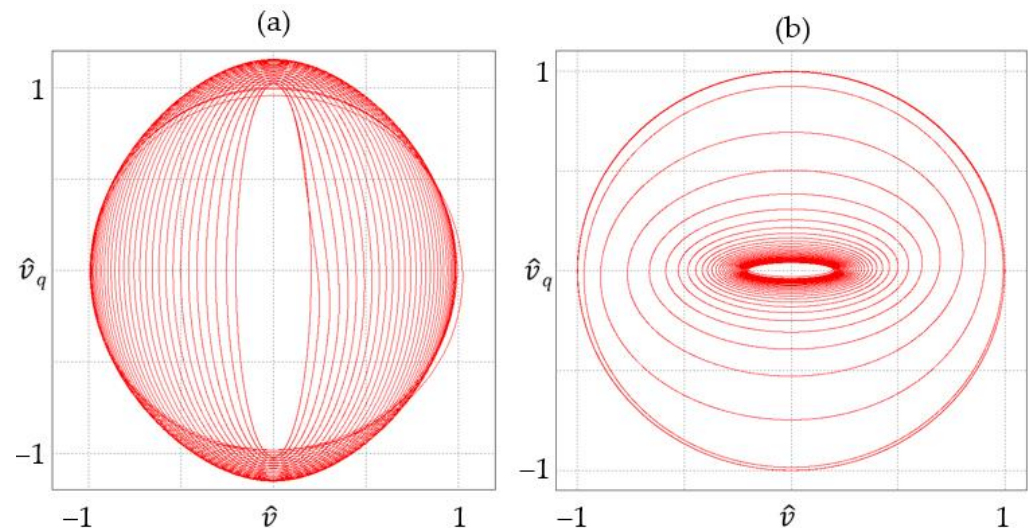


Figure 7. Trajectory of quadrature signals formed in the generalized second-order integrator for (a) $\omega = 500$ Hz, (b) $\omega = 100$ Hz.

If a known frequency change profile is substituted in place of a fixed parameter, the resulting trajectories are similar to circular trajectories. Path densities occur in the boundary of a single circle. As a consequence, it can be confirmed that the obtained quadrature waveforms will be correct during the analyzed time interval, and the amplitude and phase changes will be transient. This case such the trajectory is shown in Figure 8.

Due to the requirement of unit amplitude for quadrature signals, the approach presented for the implementation of the PLL system will result in errors in the calculation of the active and reactive components of the reference current.

This paper proposes a new quadrature signal generation method based on a generalized second-order integrator. The use of a known frequency variation profile does not give the desired effect of a circular trajectory, so the traditionally used PLL system was replaced by a reference shape signal generation (RSG) system. If the sinusoidal input signal is frequency modulated, then during the period of the signal, a change in the value of the characteristic frequency in the second-order integrator will always result in a deformation of the signal from the desired shape. To achieve the condition of unit amplitude condition with the correct phase shift, a method of synchronous latching of the current frequency value was used. Using this approach, where the current frequency value is latched for a time corresponding to the period of the input signal, will make the calculation of quadrature

signals take place with a quasi-stationary parameter corresponding to the characteristic frequency of the second-order integrator.

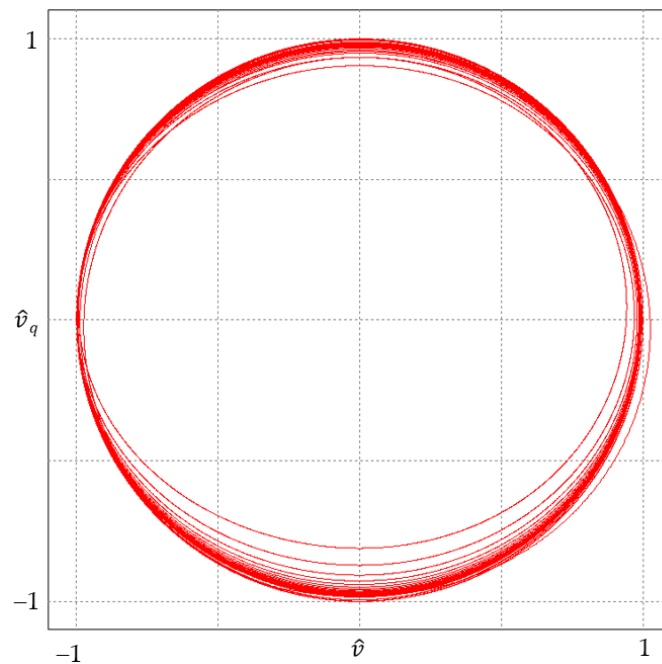


Figure 8. Trajectory of quadrature signals formed in a generalized second-order integrator for a given frequency variation profile.

Figure 9 shows a flow chart of the proposed characteristic frequency reference system.

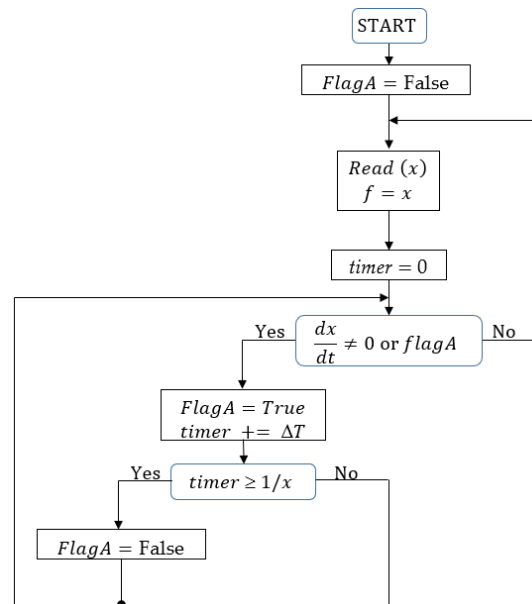


Figure 9. Flow chart of the proposed characteristic frequency reference system.

The proposed solution to the problem of changing the fixed transmittance parameter of the reference signal was based on a single-flag system. Systems based on flags are classic synchronization mechanisms that are used in concurrent programming. Their primary goal is to manage access to shared resources among multiple threads to prevent conflicts and ensure correct cooperation. The assumed binary flag (*FlagA*) is set when the frequency change trajectory (*x*) is changed. At this point, the timer is reset; after that, the interval is

measured, which is derived from the latched period value resulting from the set trajectory of frequency changes. The timer used measures time with a resolution resulting from the set interval ΔT . After measuring the current value of the reference waveform, the frequency value is updated and the new value is read from the set trajectory (x). To properly work with the algorithm shown in Figure 9, the time relations associated with the calculations performed must be met. These relations are shown in Figure 10.

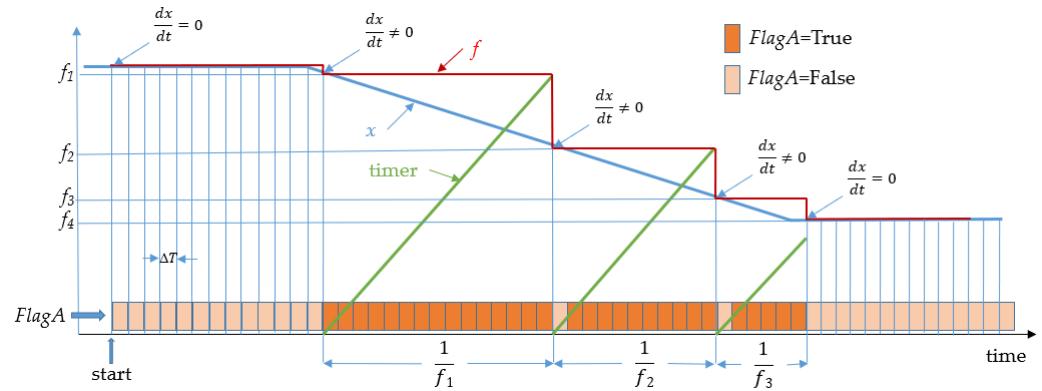


Figure 10. Graphic illustration describing the adaptive zero-order hold block process.

Taking into account the proposed frequency change adaptation system explained in Figure 10, the RSG system can be depicted as in Figure 11. In the shown system, a pre-set frequency change trajectory is input to the quadrature signal generator via an adaptive zero-order hold block (AZOH). AZOH samples the input trajectory x with varying frequency and holds the sampled value until the next synchronization cycle. The set frequency trajectory is marked in Figure 11 as the red x waveform, and the resulting frequency is marked blue as the f waveform.

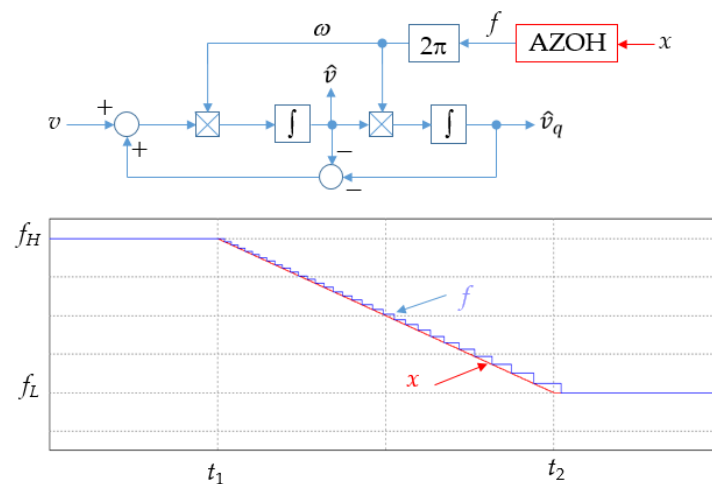


Figure 11. Structure of the RSG system and waveforms describing the operation of AZOH.

Taking into account the quadrature signals obtained from the proposed system, the waveform of the signal modulating the operation of the inverter switches was calculated using the proportional-resonant control algorithm. A diagram of the complete control system is shown in Figure 12.

The control system of the grid inverter consists of three main structures to control the current with respect to a linearly varying frequency. A proportional-integral controller (PI2), which calculates the reference value of the ac component of the inverter current (i_{ar}), is directly responsible for maintaining a constant voltage on Bus 1 (v_{DC}). According to Equation (3), the reference current of the inverter is determined, taking into account

its reactive component (i_{rr}). The reactive component is established by the higher-level system. The reference waveform of the inverter current is controlled in the proposed controller (P + R), with its output (y) fed to the inverter modulator. In typical applications of proportional-resonant controllers, its settings depend on the resonant frequency, which corresponds to the frequency of the generated waveforms in the inverter. When the frequency changes, the proposed controller automatically adjusts as a function of f . This function is calculated in the RSG structure. The RSG consists of a generalized second-order integrator (SOGI), which is described by Equations (16) and (17); an adaptive block (AZOH), which operates according to the diagram shown in Figure 9; and a frequency trajectory generator (GT). GT is a structure to generate trajectories based on the status of the O_3 signal, as shown in Figure 2. This trajectory is used in the adaptive tuning process of the controller and SOGI system and is involved in the control of the main generator through the control system (GC). The operation of the GC system is a separate issue and will not be discussed in this article.

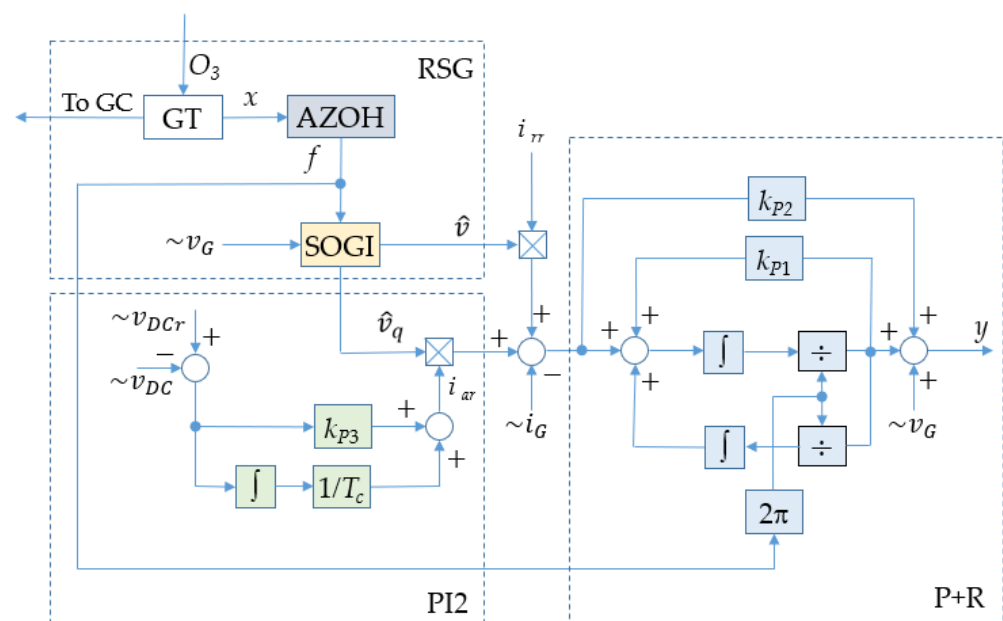


Figure 12. The proposed system of adaptive regulation of the grid converter.

3. Results

The grid inverter control system structure proposed in this article to support a power system based on a variable frequency voltage generator was described in the hardware description language (VHDL, standards IEEE 1076-1987, IEEE 1076-1993 and partially IEEE 1076-2000), which implemented it in a control board containing a reconfigurable FPGA type EP2C20F487 logic chip (Intel FPGA Corporation, previously Altera, Santa Clara, CA, USA). By using the capabilities of the VHDL language, the developed (in Quartus II, ver 9.0 software) structure was capable of running as independent instances that executed concurrently.

The tests carried out focused mainly on demonstrating the effects of the changes made to the structure of the synchronization system and on showing the impact of the proposed adaptive mechanism on the entire on-board subsystem. Therefore, the PV roles in this study were performed by a PV emulator using the Sandia model of PV modules. The tests used the debugging and visualization tools built into the FPGA chip's operating environment for on-chip signals, which communicated with the host system through a JTAG (standard IEEE 1149.1) interface. The inverter was carried out on a test bench, shown in Figure 13.

The converter control system in Figure 12 was tuned according to the settings summarized in Table 1.



Figure 13. Test stand designed for testing grid-tied inverters.

Table 1. Control system parameters.

PI	PI2	P + R
$k_p = 1$ $T_C = 0.1$	$k_{p3} = 1$ $T_C = 0.01$	$k_{p1} = 0.01$ $k_{p2} = 6.5$

3.1. RSG Tests

Tests of the RSG system were carried out to validate the proposed adaptation of a synchronizer based on a generalized second-order integrator operating at changing frequency. Figure 6 shows that the knowledge of the change in frequency trajectory alone is not sufficient for the SOGI system to correctly reproduce orthogonal unit signals. After the implementation of the AZOH system, the trajectory shown in Figure 14 was obtained.

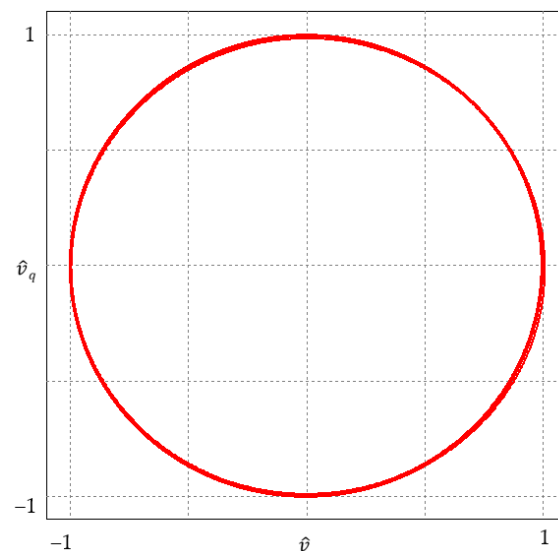


Figure 14. Trajectory of quadrature signals formed in a generalized second-order integrator for a proposed RSG with AZOH.

When comparing for the same conditions the obtained trajectory of quadrature signals, including AZOH (Figure 14) with the trajectory obtained for SOGI without the frequency trajectory adaptive system (Figure 8), it can be concluded that the obtained signals are unitary sinusoidal signals and are orthogonal. During the full profile of frequency changes, the trajectory for AZOH maintains a circular profile that generates overlapping paths. The minor variations are due to computational errors and are of marginal significance.

The tests were carried out in case of a linear frequency change from 500 to 100 Hz over a duration of 100 milliseconds.

3.2. Tests for Different Dynamics of Frequency Changes

Analysis of the performance of the proposed system to adapt the synchronization system to changing frequency leads to the conclusion that the quality of quadrature signal estimation can be affected by the slowness of the linear frequency change. To experimentally confirm this statement, synchronization systems were designed, during which the frequency change was changed from 500 to 100 Hz. For comparison purposes, the maximum deviation of the quadrature signal from the singular value was measured for the generalized second-order integrator with the set frequency profile and with the AZOH system.

The first test was carried out for a linear frequency change over 280 milliseconds. The results are shown in Figure 15.

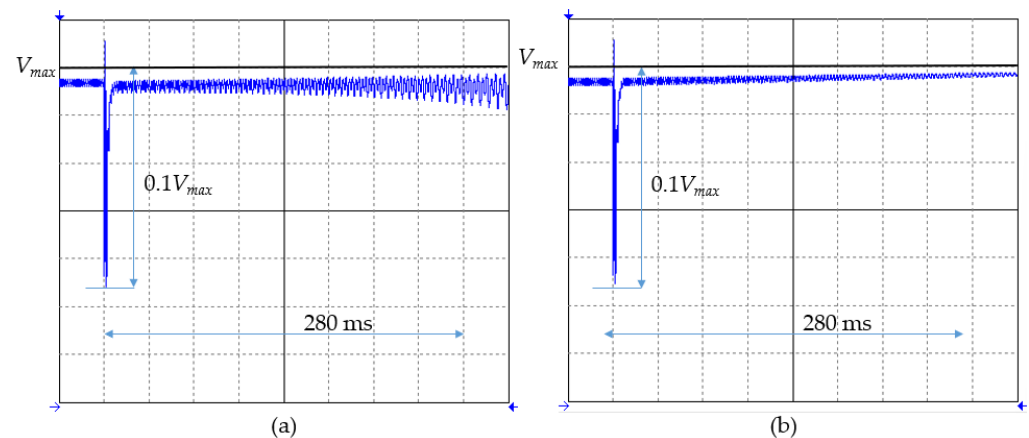


Figure 15. The trajectory modulus of quadrature signals with a frequency drop of 1.42 Hz per millisecond without (a) and with AZOH (b).

An analysis of Figure 15 shows that the largest change in the amplitude of the 0.1 amplitude quadrature signals occurs at the time of the frequency change. As can be easily deduced, this is the result of the start of the AZOH process at the time of the appearance of a non-zero value of the derivative of the frequency change. The SOGI system at a frequency change of 280 milliseconds correctly generates quadrature signals, both when the frequency change profile is entered directly (Figure 15a) and when the AZOH system was applied (Figure 15b).

Another test was performed for a frequency change of 140 milliseconds. The recorded amplitudes of the quadrature signals are shown in Figure 16.

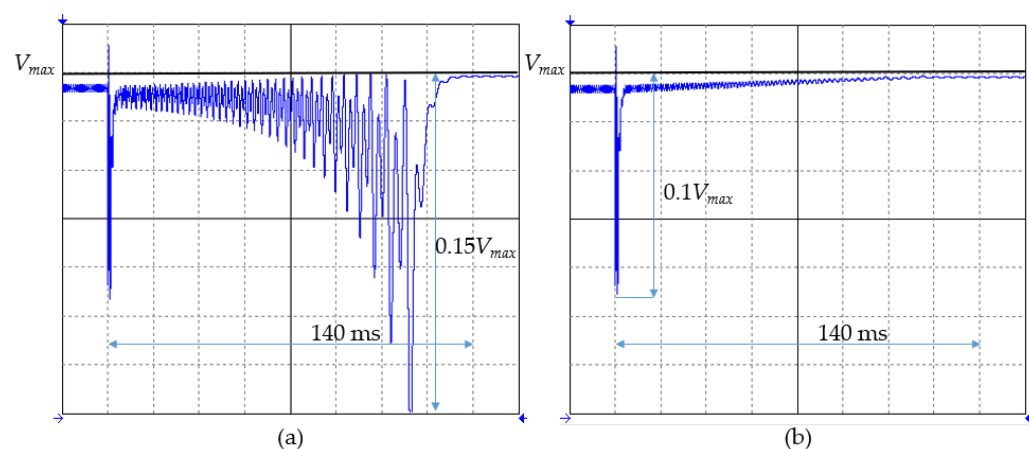


Figure 16. The trajectory modulus of quadrature signals with a frequency drop of 2.84 Hz per millisecond without (a) and with AZOH (b).

It can be seen in Figure 16 that reducing the duration of the linear frequency change by half does not affect the operation of the RSG with AZOH. The waveforms in Figures 15b and 16b are the same. When AZOH is not used in the SOGI system (Figure 16a), changes in the amplitude of quadrature signals that reach $0.85 V_{max}$ appear. Also, it should be noted that the amplitude changes continue for the entire duration of the frequency reduction.

The last recorded case refers to the duration of the frequency changes of 30 milliseconds. The results obtained for such frequency reduction conditions are shown in Figure 17.

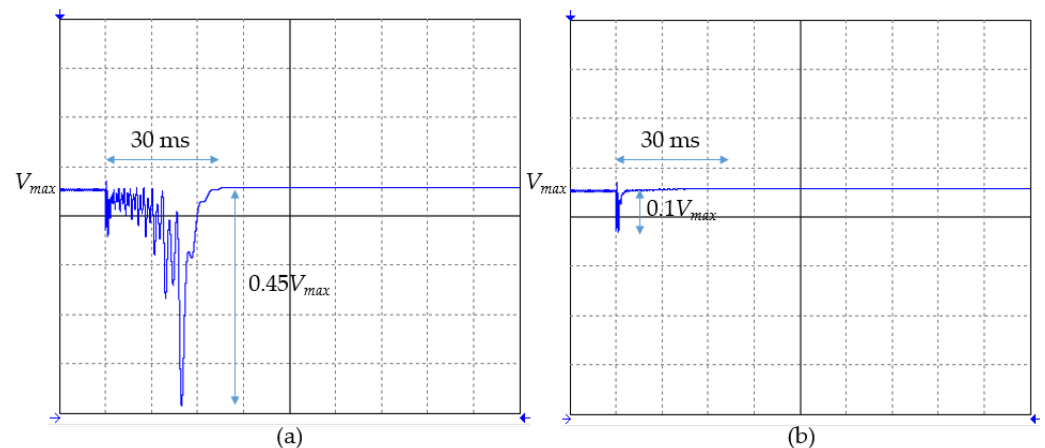


Figure 17. The trajectory modulus of quadrature signals with a frequency drop of 13.3 Hz per millisecond without (a) and with AZOH (b).

The analysis of Figure 17 confirms the effectiveness of the AZOH system even for extremely dynamic frequency variation profiles. The behavior of the RSG system with AZOH confirms the effectiveness of the system's operation. In the absence of an adaptation mechanism, for frequency changes lasting 30 milliseconds, the synchronization system reduces the amplitudes of the quadrature signals by close to 50%. In such a situation, it should be assumed that the control system will not be able to properly control the active and reactive components, which can consequently lead to emergency conditions.

Summarizing the studies performed on the influence of the dynamics of frequency profile changes, it was deduced that for slow frequency changes sustained for more than 280 milliseconds, the system with and without AZOH gives similar results. The deviations of the quadrature signals from unity are due to the amplitude characteristics of the generalized second-order integrator and the frequency reduction time. The dependence of the percentage change in the amplitude of the quadrature signal on the steepness that describes the linear frequency reduction is shown in Figure 18. When AZOH is used, the maximum value of the percentage reduction in amplitude is 10%, and it occurs only in one period. In the remaining duration of the frequency changes, the reduction in amplitude is negligibly small.

3.3. Dynamic Tests of Quadrature Signal Generator

The application of a generalized second-order integrator in a synchronization system with the proposed AZOH requires standard tests designed for PLL systems. In this study, tests were carried out for frequency step change and phase angle step change. Since the designed synchronizer operates in a system where, as a result of the ozoniser power process, the voltage frequency changes dynamically (Figure 2), tests were conducted for a constant voltage frequency and a linearly changing voltage frequency. Figure 19a shows the response of the synchronizer in the form of quadrature signals \hat{v} and \hat{v}_q for a step change in the frequency of the input signal v_i from 300 to 500 Hz. Due to the use of AZOH, no significant disturbance is observed in the output signals. During the operating mode of the system, when the frequency of the input waveform is linearly reduced and a step change in frequency to 100 Hz occurs at the time of the disturbance, the reference waveforms establish

steady-state within a period. This situation is shown in Figure 19c. The investigated system was also tested for a step change in phase angle. Tests were performed for a step change in phase angle of $\pi/3$ at a constant input signal frequency of 500 Hz. The recorded waveforms are shown in Figure 19b. Figure 19d shows the signals recorded with a phase angle step change of $\pi/3$ during linear frequency reduction in the input waveform. Similar to the tests for frequency step change, in the case of phase angle step change, the waveforms establish steady state in a time shorter than the one period of the input signal. The response time of the system is characteristic of second-order integrators due to its dynamics.

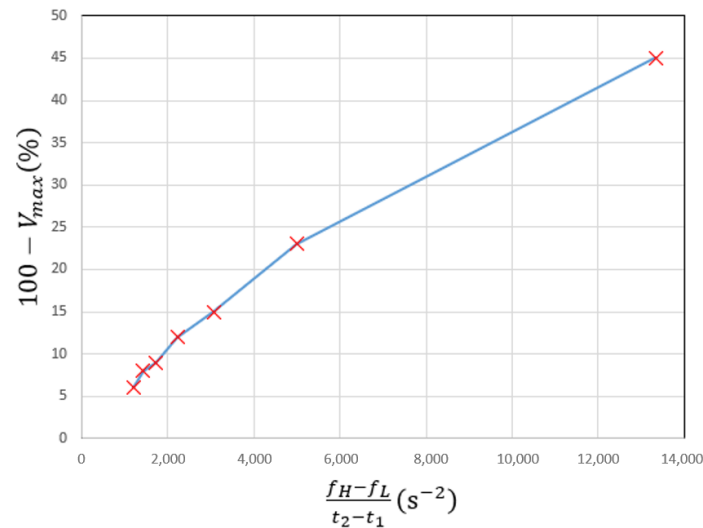


Figure 18. Percentage change in amplitude of the quadrature signal versus steepness of frequency change.

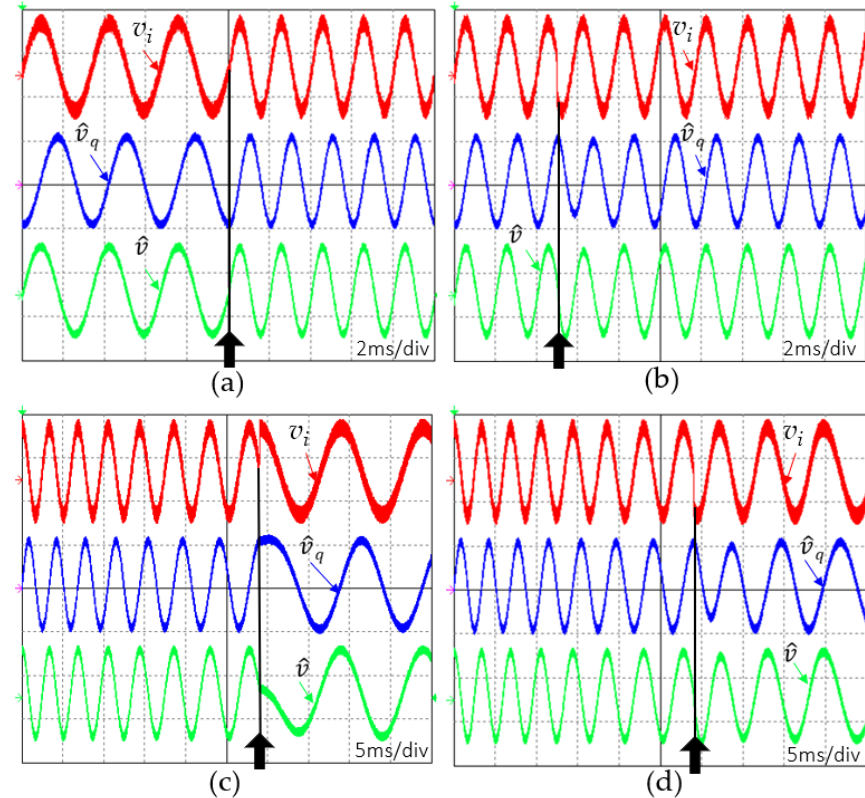


Figure 19. Response of the synchronizer in the form of quadrature signals \hat{v} and \hat{v}_q to the input signal v_i for: step change in the frequency of the input signal (a); step change in the phase angle (b); step change in the frequency during its linear reduction (c); step change in the phase angle during frequency reduction (d).

The developed synchronization system was also tested for an input signal disturbed by the third harmonic with an amplitude equal to 20% of the amplitude of the fundamental component. The response of the system is shown in Figure 20a. In this case, the shape of the quadrature signals is deformed insignificantly, which results directly from the Bode plots of the generalized second-order integrator presented in Figure 4. If the input signal was disturbed by white noise of unit amplitude, the properties of the second-order integrator effectively eliminate it from the output waveforms. This case is demonstrated in Figure 20b.

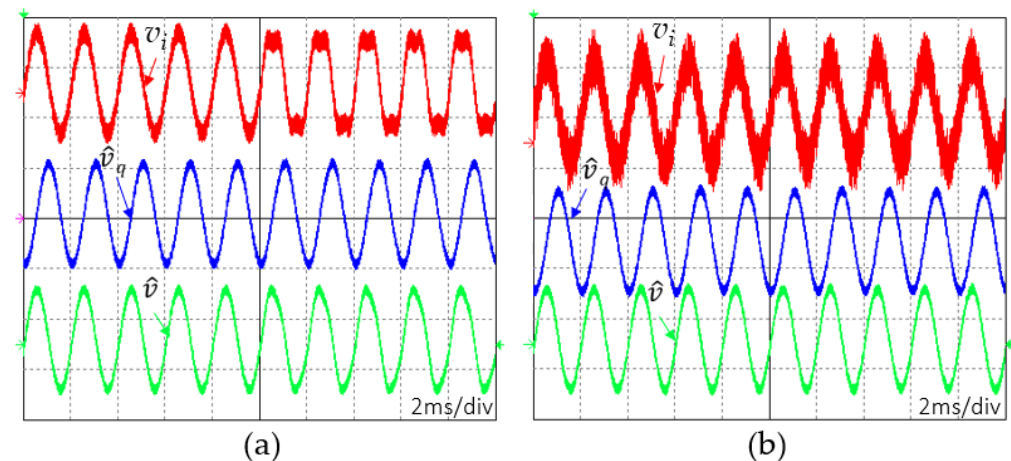


Figure 20. Response of the synchronizer in the form of quadrature signals \hat{v} and \hat{v}_q for: fundamental component v_i disturbed by the third harmonic (a); fundamental component v_i disturbed by the white noise (b).

3.4. Tests of the Power System

The control system shown in Figure 12, implemented in a control board with an FPGA, was tested on a test bench with a grid inverter connected to the existing power line depicted as Bus 2. The parameters of the power line connected generator to the ozoniser are: $R = 0.24 \Omega$ and $L = 80 \mu\text{H}$ and results from the specific construction of the power system. Tests were carried out on the effect of the proposed RSG on the precision of reconstructing the reference values of the active and reactive components of the grid current in the set trajectories of changes in the amplitude and frequency of the voltage at Bus 2. The tests carried out concern two cases:

1. The set active component with zero reactive component;
2. The set active component equal to the reactive component (phase angle of 45 degree).

Figure 21 shows the waveform of the grid inverter current and voltage registered on Bus 2 with a non-zero set active component and a zero reactive component. From the analysis of the results, it can be seen that in all start-up states, including voltage rise at constant frequency, linear frequency reduction, and steady state, the current waveforms are in phase with the voltage waveform.

Figure 22 shows the current and voltage waveforms recorded for a given inverter current that contains active and reactive components with the same values. Consequently, the current flowing from the photovoltaic system into Bus 2 should have a phase shift of 45 degrees.

The power circuit confirmed the effectiveness of the proposed adaptive synchronization method that implements the AZOH algorithm in the RSG. In addition, information about the change in the frequency of the voltage on Bus 2 was used in the control of controlling the output current of the grid inverter. Consequently, the possibility of regulating the active and reactive components of the inverter current was also obtained in states of dynamically changing voltage frequency.

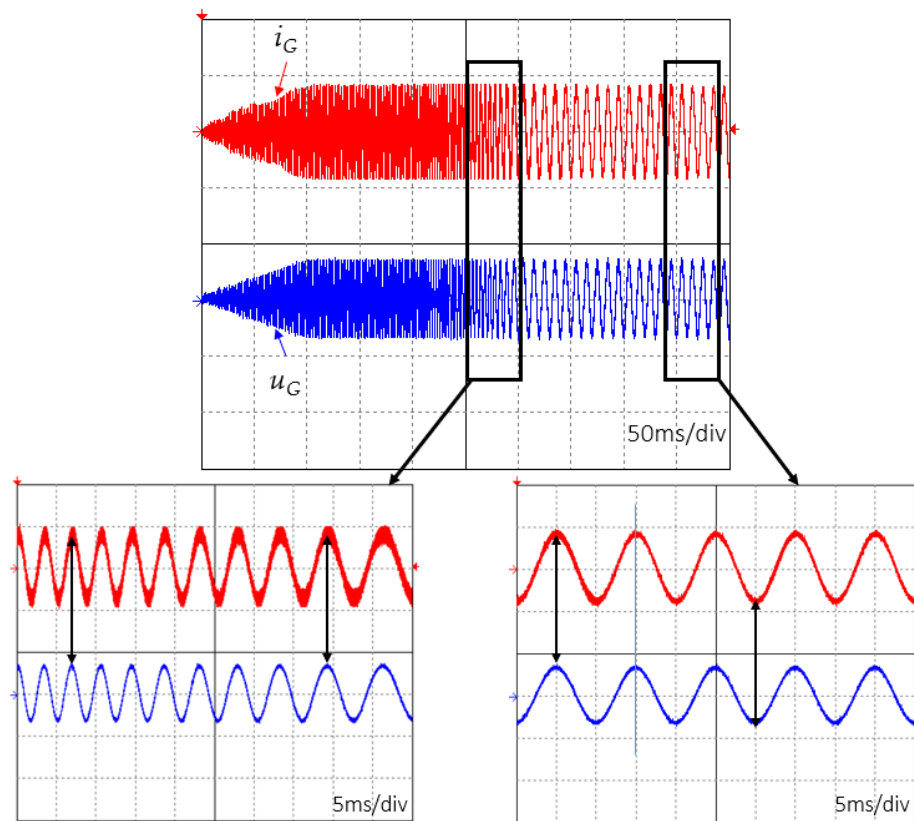


Figure 21. Current and voltage waveforms of the mains inverter measured on Bus 2 with non-zero active component and zero reactive component.

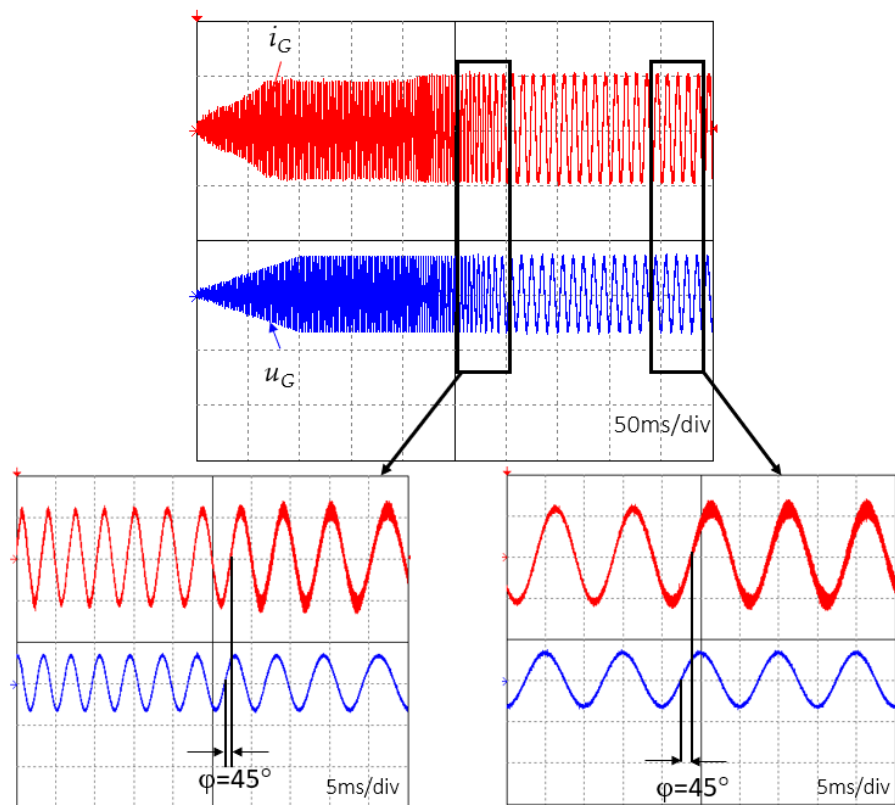


Figure 22. Current and voltage waveforms of the mains inverter measured on Bus 2 with the same active and reactive component.

4. Conclusions

This paper has proposed a single-phase converter system connected to an on-board bus with a changing voltage frequency. During dynamic voltage frequency variation, standard synchronizers based on generalized second-order integrators cannot maintain unit amplitudes of quadrature signals, which are necessary for accurate control of active and reactive power. By implementing the proposed adaptive procedure, unitary synchronization signals with a known frequency variation profile are obtained while adapting the resonant frequencies of the grid current controller. Analytically, it is shown that the dynamics of voltage frequency changes has a key effect on the accuracy of quadrature signal estimation. In the proposed method, the rate of change does not play a significant role in the estimation of synchronization signals, making it possible to control active and reactive power even at high dynamics and with a wide range of voltage frequency changes. In this study, it was shown that the application of direct adaptation does not give the expected results, as it causes changes in the modulus of the quadrature trajectories of the reference signals. Only the use of the author's solution in the form of AZOH makes it possible to maintain the reference circular trajectory for different frequencies and during its change. Due to the use of the PV panel emulator in the research, in which a Sandia model is used, the sharp decrease in frequency can be possible as an effect of the PV modeling. Future studies are to be carried out on the effect of the PV model accuracy on the dynamics of possible frequency changes.

Author Contributions: Conceptualization, T.B.; methodology, T.B.; software, T.B.; validation, T.B., L.B. and D.M.; formal analysis, T.B.; investigation, T.B. and L.B.; resources, T.B., D.M. and P.P.; data curation, T.B., L.B., D.M. and P.P.; writing—original draft preparation, T.B.; writing—review and editing, T.B. and P.P.; visualization, T.B. and L.B.; supervision, T.B.; project administration, T.B.; funding acquisition, T.B. All authors have read and agreed to the published version of the manuscript.

Funding: This research and the APC were funded by the Minister of Education and Science of the Republic of Poland "Maintain the research potential of the discipline of automation, electronics and electrical engineering", grant number: PB22.EE.24.001.

Data Availability Statement: The original contributions presented in this study are included in the article. Further inquiries can be directed to the corresponding author.

Acknowledgments: The research was carried out at the Department of Electric Power Engineering, Faculty of Electrical Engineering and Informatics, Technical University of Kosice, in relation to a research internship. The authors thank the management of the department for providing research workstations.

Conflicts of Interest: The authors declare no conflicts of interest.

References

1. Luke, M.; Jenkins, J.; Thernstrom, S. Deep Decarbonization of the Electric Power Sector: Insights from Recent Literature. *Environmental Science, Engineering*. 2017. Available online: <https://api.semanticscholar.org/CorpusID:198756972> (accessed on 10 December 2024).
2. Rohten, J.; Espinoza, J.; Villarroel, F.; Perez, M.; Munoz, J.; Melin, P.; Espinoza, E. Static power converter synchronization and control under varying frequency conditions. In Proceedings of the IECON 2012—38th Annual Conference on IEEE Industrial Electronics Society, Montreal, QC, Canada, 25–28 October 2012; pp. 786–791. [CrossRef]
3. Sajadi, A.; Kenyon, R.W.; Hodge, B.M. Synchronization in electric power networks with inherent heterogeneity up to 100% inverter-based renewable generation. *Nat. Commun.* **2022**, *13*, 2490. [CrossRef] [PubMed]
4. Kenyon, R.W.; Bossart, M.; Marković, M.; Doubleday, K.; Matsuda-Dunn, M.; Mitova, S.; Julien, S.A.; Hale, E.T.; Hodge, B. Stability and control of power systems with high penetrations of inverter-based resources: An accessible review of current knowledge and open questions. *Sol. Energy* **2020**, *210*, 149–168. [CrossRef]
5. Kenyon, R.W.; Sajadi, A.; Bossart, M.; Hoke, A.; Hodge, B.M. Interactive Power to Frequency Dynamics Between Grid-Forming Inverters and Synchronous Generators in Power Electronics-Dominated Power Systems. *IEEE Syst. J.* **2023**, *17*, 3456–3467. [CrossRef]
6. Cho, C.; Jeon, J.H.; Kim, J.Y.; Kwon, S.; Park, K.; Kim, S. Active Synchronizing Control of a Microgrid. *IEEE Trans. Power Electron.* **2011**, *26*, 3707–3719. [CrossRef]
7. Tripathy, P.; Misra, B.; Nayak, B. Phase-locked loop based synchronization schemes for three-phase unbalanced and distorted grid: A review. *Int. J. Appl. Power Eng. IJAPE* **2024**, *13*, 934. [CrossRef]

8. Shinnaka, S.A. Robust Single-Phase PLL System With Stable and Fast Tracking. *Trans. Ind. Appl.* **2008**, *44*, 624–633. [\[CrossRef\]](#)
9. Salamah, A.M.; Finney, S.J.; Williams, B.W. Three-phase phase-lock loop for distorted utilities. *IET Electr. Power Appl.* **2007**, *1*, 937–945. [\[CrossRef\]](#)
10. Timbus, A.V.; Teodorescu, R.; Blaabjerg, F.; Liserre, M.; Dell’Aquila, A. Independent Synchronization and Control of Three Phase Grid Converters. In Proceedings of the International Symposium on Power Electronics, Electrical Drives, Automation and Motion-SPEEDAM 2006, Taormina, Italy, 23–26 May 2006; pp. 1246–1251.
11. Robles, E.; Ceballos, S.; Pou, J.; Martín, J.L.; Zaragoza, J.; Ibañez, P. Variable-Frequency Grid-Sequence Detector Based on a Quasi-Ideal Low-Pass Filter Stage and a Phase-Locked Loop. *IEEE Trans. Power Electron.* **2010**, *25*, 2552–2563. [\[CrossRef\]](#)
12. Chung, S. Phase-locked loop for grid-connected three-phase power conversion systems. *IEE Proc.-Electr. Power Appl.* **2000**, *147*, 213–219. [\[CrossRef\]](#)
13. Moreno, V.M.; Liserre, M.; Pigazo, A.; Dell’Aquila, A.A. Comparative Analysis of Real-Time Algorithms for Power Signal Decomposition in Multiple Synchronous Reference Frames. *IEEE Trans. Power Electron.* **2007**, *22*, 1280–1289. [\[CrossRef\]](#)
14. Huang, C.H.; Lee, C.H.; Shih, K.J.; Wang, Y.J. Frequency Estimation of Distorted Power System Signals Using a Robust Algorithm. *IEEE Trans. Power Deliv.* **2008**, *23*, 41–51. [\[CrossRef\]](#)
15. Agha Zadeh, R.; Ghosh, A.; Ledwich, G. Combination of Kalman Filter and Least-Error Square Techniques in Power System. *IEEE Trans. Power Deliv.* **2010**, *25*, 2868–2880. [\[CrossRef\]](#)
16. Huang, C.; Lee, C.; Shih, K.; Wang, Y. Frequency Estimation of Distorted Power System Signals Using Robust Extended Complex Kalman Filter. In Proceedings of the Intelligent Systems Applications to Power Systems, Kaohsiung, Taiwan, 5–8 November 2007; pp. 1–6. [\[CrossRef\]](#)
17. Džafić, I.; Jabr, R. Discrete-time analytic signals for power system phasor and frequency tracking. *Int. J. Electr. Power Energy Syst.* **2023**, *148*, 109003. [\[CrossRef\]](#)
18. Lavopa, E.; Zanchetta, P.; Sumner, M.; Cupertino, F. Real-Time Estimation of Fundamental Frequency and Harmonics for Active Shunt Power Filters in Aircraft Electrical Systems. *IEEE Trans. Ind. Electron.* **2009**, *56*, 2875–2884. [\[CrossRef\]](#)
19. Sok, V.; Kim, S.-H.; Lak, P.Y.; Nam, S.-R. A Novel Method for Removal of Dual Decaying DC Offsets to Enhance Discrete Fourier Transform-Based Phasor Estimation. *Energies* **2024**, *17*, 905. [\[CrossRef\]](#)
20. Prakash, S.; Singh, J.K.; Behera, R.L.; Mondal, A. Comprehensive Analysis of SOGI-PLL Based Algorithms for Single-Phase System. In Proceedings of the 2019 National Power Electronics Conference (NPEC), Tiruchirappalli, India, 13–15 December 2019; pp. 1–6. [\[CrossRef\]](#)
21. Kalkoul, S.; Benalla, H.; Nabti, K.; Reama, A. Comparison Among Single-phase PLLs Based on SOGI. In Proceedings of the 2020 6th International Conference on Electric Power and Energy Conversion Systems (EPECS), Istanbul, Turkey, 5–7 October 2020; pp. 118–122. [\[CrossRef\]](#)
22. Stojic, D.; Tarczewski, T.; Niewiara, L.J.; Grzesiak, L.M. Improved Fixed-Frequency SOGI Based Single-Phase PLL. *Energies* **2022**, *15*, 7297. [\[CrossRef\]](#)
23. Fan, M.; Dai, Z.; Yang, Y.; Xie, M.; Zhao, P.; Zhang, J. Fast grid synchronization method for variable-frequency AC systems. *Int. J. Electr. Power Energy Syst.* **2020**, *120*, 105990. [\[CrossRef\]](#)
24. Teodorescu, R.; Liserre, M.; Rodriguez, P. *Grid Converters for Photovoltaic and Wind Power Systems*; Wiley: Hoboken, NJ, USA, 2011.
25. Dai, Z.; Qiu, Y.; Li, J.; Zhang, C. Global asymptotic estimation of grid voltage parameters for variable frequency AC systems. In Proceedings of the IECON 2017—43rd Annual Conference of the IEEE Industrial Electronics Society, Beijing, China, 29 October–1 November 2017; pp. 4155–4159. [\[CrossRef\]](#)
26. Binkowski, T.; Nowak, M.; Piróg, S. Power Supply and Reactive Power Compensation of a Single-Phase Higher Frequency On-Board Grid with Photovoltaic Inverter. *Energies* **2022**, *15*, 2563. [\[CrossRef\]](#)
27. Feroz Mirza, A.; Mansoor, M.; Ling, Q.; Khan, M.I.; Aldossary, O.M. Advanced Variable Step Size Incremental Conductance MPPT for a Standalone PV System Utilizing a GA-Tuned PID Controller. *Energies* **2020**, *13*, 4153. [\[CrossRef\]](#)

Disclaimer/Publisher’s Note: The statements, opinions and data contained in all publications are solely those of the individual author(s) and contributor(s) and not of MDPI and/or the editor(s). MDPI and/or the editor(s) disclaim responsibility for any injury to people or property resulting from any ideas, methods, instructions or products referred to in the content.